Heliyon 10 (2024) e36597

Contents lists available at ScienceDirect

Heliyon

journal homepage: www.cell.com/heliyon

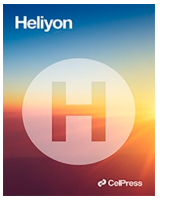

Research article

The tumorigenic effect of the high expression of ABRACL in glioma and its potential as a therapeutic target

Chenhui Zhao [a], Zeyu Wu [b], Zhipeng Yao [c], Fan Zhang [c], Rui Zhao [b], Xiaoxiang Cao [b], Shizhang Ling [b], Xiaochun Jiang [a,*]

[a] *Department of Neurosurgery, Shandong Provincial Third Hospital, Shandong University, Jinan, China*
[b] *Translational Research Institute for Neurological Disorders, The First Affiliated Hospital of Wannan Medical College (Yijishan Hospital of Wannan Medical College), Wannan Medical College, Wuhu, China*
[c] *School of Chemistry and Chemical Engineering, Southeast University, Nanjing, China*

A B S T R A C T

Gliomas are the most common malignant intracranial tumors, with no effective treatments. Better understanding and identification of novel targets are urgently warranted. Actin-binding Rho activating C-terminal like (ABRACL) has been reported as an oncogene in several cancer types. However, the potential roles of ABRACL in the tumorigenesis of malignant glioma remain unknown. We discovered that ABRACL is highly expressed in different sub-types of gliomas in both CGGA and TCGA databases, which was further validated in glioblastoma cell lines and normal human astrocyte lines. RT-qPCR, Western blotting and immunohistochemistry demonstrated that ABRACL expression in glioma tissues was upregulated along with the increasing WHO grades. Further survival analysis of glioma patients also revealed that the overall survival of patients in the ABRACL high expression level group were significantly shorter than those in the low expression level group. Knockdown of ABRACL inhibited the proliferation, cell migration, invasion and cytodynamics behaviors in glioma cell lines via activating STAT3 signaling, which also induced apoptosis and cell cycle arrest. Conversely, overexpressing ABRACL promoted cell renewing and migration, enabled more flexible cell deformation, supporting ABRACL being a bona fide oncogene. Intracranial orthotopic xenograft experiment further confirmed that ABRACL downregulation significantly suppressed glioma growth. These results have demonstrated that the tumorigenic effect of ABRACL is partly mediated by STAT3, whose expression also correlates with clinical prognosis. ABRACL facilitates glioma malignancy phenotype through regulating the cytoskeleton by activating STAT3 pathway, suggesting that it may represent a potential therapeutic target for glioblastoma.

1. Introduction

Glioma is the most common and aggressive intracranial malignant tumor [1], with spontaneous, infiltrating, and recurring essences [2,3]. The fatality rate is only second to lung and pancreatic cancer among various tumor types in all parts of the human body. High-grade glioma, especially glioblastoma multiforme (GBM), has a higher incidence, poorer prognosis and shorter median survival time, of which the 5-year survival rate does not exceed 5 % [4,5]. Malignant glioma is an important scientific mystery of the central nervous system tumors to be solved urgently [6,7]. However, traditional treatment methods, including surgical resection, radiotherapy, and chemotherapy have reached the "limit" in terms of prolonging the survival time of patients, during the past decades [8,9]. Thus, new strategies to provide novel targets and discover key players related to the occurrence, development, and recurrence of glioma are imminently warranted.

Actin-binding Rho activator protein C-terminal like protein (ABRACL) gene belongs to a new family of low molecular weight proteins, located on chromosome 6p24.1, consisting of 81 amino acid proteins [10]. Recent studies supported that the actin-associated

* Corresponding author.
E-mail address: jiangxiaochun2019@hotmail.com (X. Jiang).

https://doi.org/10.1016/j.heliyon.2024.e36597
Received 16 February 2024; Received in revised form 19 August 2024; Accepted 19 August 2024
Available online 28 August 2024
2405-8440/© 2024 The Authors. Published by Elsevier Ltd. This is an open access article under the CC BY-NC license (http://creativecommons.org/licenses/by-nc/4.0/).

Abbreviations list

A	Astrocytoma
AA	Anaplastic astrocytoma
ABRACL	Actin-binding Rho activating C-terminal like
ANOVA	One-way analysis of variance
AO	Anaplastic oligodendroglioma
Bax	BCL2-Associated X
CCGA	Chinese Glioma Genome Atlas
CCK-8	Cell counting kit-8
CD4	Cluster of differentiation 4
cDNA	Complementary DNA
CDS	Codingsequence
Codel	Co-deletion
DAB	Diaminobenzidine
DAPI	4′,6-diamidino-2-phenylindole
DEG	Differentially expressed genes
DMEM	Dulbecco's Modified Eagle's medium
H-E	Hematoxylin-Eosin
ECL	Enhanced ChemiLuminescence
EDTA	Ethylenediamine tetraacetic acid
EDU	5-ethynyl-2-deoxyuridine
FBS	Fetal bovine serum
FITC	Fluorescein isothiocyanate
GAPDH	Glyceraldehyde-3-phosphate dehydrogenase
GBM	Glioblastoma multiforme
GO	Gene Ontology
GTP	Guanosine triohosphte
HA	Human astrocyte cell line
HEK293T	Human embryonic kidney cell line
IDH	Isocitrate dehydrogenase
IHC	Immunohistochemistry
IL-2/STAT5	Interleukin-2/transcription 5
IRS	Immunoreactivity score
JAK/STAT3	Janus kinase/transcription 3
KEGG	Kyoto Encyclopedia of Genes and Genomes
KM	Kaplan–Meier
KPS	Karnofsky Performance Status Scale
K-RAS	Rat sarcoma genes
LGG	Low grade glioma
LV-ABRACL	ABRACL over-expression group
LV-Ctrl	Positive control group
MMP 2	Matrix Metallopeptidase 2
MMP 9	Matrix Metalloproteinase 9
O	Oligodendroglioma
OS	Overall survival
PBS	Phosphate buffered saline
PI	Propidium iodide
PRS	Primary, recurrent, or secondary
PVDF	Polyvinylidene fluoride
qRT-PCR	Quantitative real-time polymerase chain reaction
Ra	Recurrent astrocytoma
rAA	Recurrent anaplastic astrocytoma
rGBM	Recurrent glioblastoma
RNA	RibonucleicAcid
RNA-seq	RNA sequencing
rO	Recurrent oligodendroglioma
SD	Standard deviation
SDS-PAGE	Sodium dodecyl sulfate-polyacrylamide gel electrophoresis
sGBM	Secondary glioblastoma

Sh-ABRACL	ABRACL knockdown group
ShRNA	Short hairpin RNA
STAT3	Signal Transducer And Activator Of Transcription 3
TCGA	The Cancer Genome Atlas
TNF-α	Tumour Necrosis Factor alpha
TRITC	Tetramethylrhodamine
TRIzol	TRI reagent
WHO	World Health Organization

proteins can directly influence tumor's progression in different types of tumor cells [11–13]. The main function of ABRACL is to regulate muscle kinetic protein dynamics and cell movement [14]. Lin et al. discovered that ABRACL can facilitate cell motility and actin dynamics [10]. Ura et al. concluded that the expression of ABRACL gene was also up-regulated in endometrial cancer through analyzing the proteomics of endometrial cancer and normal control tissues [15]. Several other studies reported that ABRACL can predict short relapse-free survival and worse overall survival of gastric cancer patients and that increased expression of ABRACL played a crucial role in its distant metastasis of gastric cancer [16]. Furthermore, accumulating evidence has demonstrated that ABRACL is closely related to the occurrence, invasion and metastasis of esophageal carcinoma, colon cancer and other tumors [17–19]. Our previous study demonstrated that Rhoj, a member of Rho GTPase family, promoted GBM progression via cytodynamics pathway [20]. All of these results have revealed that ABRACL may act as an oncogenic function in cancer development. However, the exact roles of ABRACL in malignant glioma are still largely unknown. In this study, we are dedicated to investigate the relationship between ABRACL and glioma.

In the current study, we first explored the expression level, prognostic value, clinicopathological and biological functions of ABRACL in gliomas using public available datasets from TCGA and CCGA. We found that ABRACL expression in malignant gliomas was significantly higher than that of normal tissues, correlated with WHO grades, 1p/19q co-deletion status and IDH mutation status, and elevated ABRACL expression level was associated with poorer outcome and shorter survival time of glioma patients. In addition, the effects of ABRACL up- and down-regulation on proliferation, cell cycle, apoptosis, migration, invasion and cytoskeleton of glioma cells were evaluated. Importantly, we further identified that ABRACL inhibited apoptosis of glioma cells and promoted proliferation, cell cycle, migration and invasion, as well as cytoskeleton of glioma cells by activating STAT3 signaling. Moreover, ABRACL down-regulation decreased the expression levels of MMP2 and Ki-67 and suppressed glioma progression in vivo. Taken together, our findings reveal that the upregulation of ABRACL is important in maintaining pathogenesis and malignant phenotype of glioma by activating the STAT3 signaling pathway, indicating that ABRACL may represent a potential molecular target for diagnosis and treatment of malignant glioma.

2. Materials and methods

2.1. Bioinformatics

We downloaded the gene expression data and clinicopathological data of gliomas from the Chinese Glioma Genome Atlas (CGGA) (http://www.cgga.org.cn) and The Cancer Genome Atlas (TCGA) (https://www.cancergenome.nih.gov) datasets. Patients without clinical information were excluded. After screening, we obtained 817 (CGGA dataset) and 658 (TCGA dataset) glioma patients. Gene enrichment analysis was conducted using the GSVA R package to analyze differences in tumor hallmark pathways between different groups. The gene sets of "Hallmarks" were downloaded from the MSigDB database for GSVA enrichment analysis. The differentially expressed genes (DEGs) between high- and low-ABARCL groups were identified using the empirical Bayesian approach of the limma R package. The cutoff values were set as adjusted p-value <0.05 and $|Log_2FC|>1$. The clusterProfiler R package was employed to implement GO and KEGG enrichment analyses for DEGs. A set of marker genes for tumor-infiltrating immune cells was acquired from a previous study (Supplemental Fig. 1). By applying the ssGSEA, the enrichment scores of 28 immune cells for each gliomas sample were quantified based on expressed gene signatures using the GSVA R package.

2.2. Surgically resected glioma samples and cell lines

The human glioblastoma cell lines, U87-MG, T98-G and human astrocyte cell line (HA) were cultured in DMEM medium supplemented with penicillin/streptomycin (Sangon Biotech, Shanghai, China) and 10 % fetal bovine serum (FBS) (Gibco, CA, USA). All cells were cultured at 37 °C and 5 % CO_2. A total of 56 glioma tissues and 5 normal human brain specimens were collected in the First Affiliated Hospital of Wannan Medical College from May 2020 to November 2022. There were WHO grade I: 1 case, WHO grade II: 14 cases, WHO grade III: 10 cases, and WHO grade IV: 31 cases, among these 56 glioma cases. All patients were newly diagnosed of glioma, without radiotherapy or chemotherapy before surgery. This study was approved by the Ethics Committee of the First Affiliated Hospital of Wannan Medical College(WNMC-LSD-202020), and the patients had signed a written informed consent.

2.3. RNA isolation and real-time quantitative polymerase chain reaction (RT-qPCR)

Tissues or cells were lyzed using TRIzol reagent (Catalog number: 15596026, ThermoFisher Scientific, USA). The total RNA was

extracted by TRIzol RNA extraction kit (ThermoFisher Scientific, Shanghai, China). The RNA concentration was measured by NanoDrop 2000 spectrophotometer (ThermoFisher Scientific). Primers were designed by online primer design software, Primer3 (http://frodo.wi.mit.edu/primer3/). The specific primer sequence was synthesized by SANGON biotech Company (Shanghai, China). The following primers were used: ABRACL forward primer:

5′-TGAATGTGGATCACGAGGTT-3′ and ABRACL reverse primer: 5′-TCGTTTTGCAGCTTTAAGAGTTC-3'; GAPDH forward primer: 5′-TGACTTCAACAGCGACACCCA-3′ and GAPDH reverse primer:5′-CACCCTGTTGCTGTAGCCAAA-3'. The reverse transcription (RT) from total RNA to the first-strand cDNA was performed according to the instructions of RT kit (TransGen Biotech, Beijing, China). RT-qPCR reaction volume was 25 μl with each sample in triplicate and PCR reactions were carried out according to the instructions of PCR kit (TransGen Biotech, Beijing, China). The expression level of mRNA was calculated by relative quantitative method, $RQ = 2^{-\triangle\triangle Ct}$. The RT-qPCR experiment was repeated three times.

2.4. Immunohistochemical staining (IHC)

Formalin-fixed and paraffin embedded tissue sections were cut at 4 μm in thickness and then the antigen retrieval was done by steaming a container with tissue-section slides immersed in 0.01 mol/L citrate buffer (pH 6.0) for 15 min in a vegetable steamer (Midea Company, Guangzhou, China), followed with a cooling of the container at room temperature for 30 min and inactivation of endogenous peroxidase with 3 % H_2O_2 at room temperature for 10 min, then blocked with 5 % bovine serum albumin at 37 °C for 30 min, and finally incubated overnight with ABRACL antibody at a 1:400 dilution (Catalog number: PA5-56401, ThermoFisher Scientific, USA) at 4 °C. After three washes with 1X PBS, 10 min each, and then incubated with HRP-labeled goat anti-rabbit IgG polymer at room temperature for 1 h. After three washes with 1 × PBS, 10 min each, tissue sections were visualized by Diaminobenzidine (DAB), and then counterstained with hematoxylin. After tissue sections were dehydrated in a series of the increased concentrations of ethanol, and then treated in xylene. Slides were coverslipped in a neutral gum mount (KeyGen Biotech, Jiangsu, China). An H-scoring method was used to analyze the IHC staining results by taking into account of the degree of staining (negative staining, light yellow, light brown, and dark brown are counted as 0, 1, 2, and 3 points) and the range of positively stained cells in a tissue section (0, 1 %～25 %, 26 %～50 %, 51 %～75 %, 76 %～100 %, as 0–4 points, respectively). An H-score of ABRACL expression was obtained by finally multiplying these two points.

2.5. Protein extraction and western blotting

The tissue total protein was extracted at 1:25 ratio (1 mg tissue with 25 μl lysis buffer with the inhibitors of proteases and phosphatases) after weighing and the protein concentration was measured by bicinchoninic acid method. The proteins were resolved by sodium dodecyl sulfate-polyacrylamide gel electrophoresis (SDS-PAGE), after 5 μg of total protein of each sample was loaded into a well, followed by polyvinylidene fluoride (PVDF) membrane transfer (300 mA, 1 h), blocked with 5 % milk for 2 h at room temperature, and then probed with primary antibody against ABRACL (rabbit anti-human ABRACL polyclonal antibody (Catalog number: PA5-56401, Thermo Fisher Scientific, USA) or GAPDH (Sangon BioTech, Shanghai, China) overnight at 4 °C. After washing, the membrane was incubated with secondary antibody conjugated to horseradish peroxidase for 1 h at room temperature. The chemiluminescent signal was developed using an ECL kit (Catalog number: WBKLS0500, Millipore, USA) and then visualized using an Amersham ImageQuant 800 machine (Uppsala, Sweden). All experiments were repeated at least 3 times.

2.6. Construction of lentiviral-based shRNA knockdown and transfection of glioma cells

ABRACL (accession number: GIEL0329847) was knocked down by lentiviral vector-mediated transfection. Each of three short hairpin (sh) RNAs against the different regions of 5′-UTR of ABRACL mRNA (5′–3′, shABRACL#1: ATTGGTAGGAACTCTTAAA; shABRACL#2: CTCTTCCGTGATGATAAAT; shABRACL#3: CTGGTAAACTGGAATATAA) or scrambled control shRNA (TTCTCCGAACGTGTCACGT) was subcloned into GV344-puro lentiviral vector. The shRNA vectors were purchased from Genechem (Shanghai, China). Lentivirus-based vector CV146 was constructed for ABRACL overexpression by Genechem. The CDS sequence of ABRACL was sub-cloned into CV146 lentivirus-based vector, followed by packaging in HEK293T cells, and the CDS sequence of ABRACL that was subcloned into a lentivirus-based vector was verified by sequencing.Briefly, U87-MG and T98G cells were transfected with 2.0 μg lentivirus per well in 6-well plates using 5 μg/ml polybrene (Invitrogen, USA) according to the manufacturer's instructions. Fresh DMEM supplemented with 10 % FBS was added to 6-well plates after 24 h of transfection. After 72 h of transfection, the complete medium containing 2 μg/μl of puromycin was added to screen the positively infected cell clones, and the duration of screening time was 7–14 days. The stable infected cells were divided into two groups: positive control group (LV-Ctrl), ABRACL over-expression group (LV-ABRACL group), negative control group (Sh-Ctrl group, infected with control ShRNA) and ABRACL knockdown group (Sh-ABRACL group).

2.7. Cell counting kit-8 (CCK-8) assay

The proliferation ability of cells was determined by CCK-8 method. The stable transfected cells were plated in 96-well plates with 5000 cells/well; 6 wells were set for each group. After incubation for 24h, 48h and 72h, 10 μl of CCK-8 reagent were added and cells were cultured for additional 2h. The absorbance value was measured at the wave length of 450 nm with a multifunctional microplate reader (Epoch2, BioTek, USA).Three independent experiments were performed.

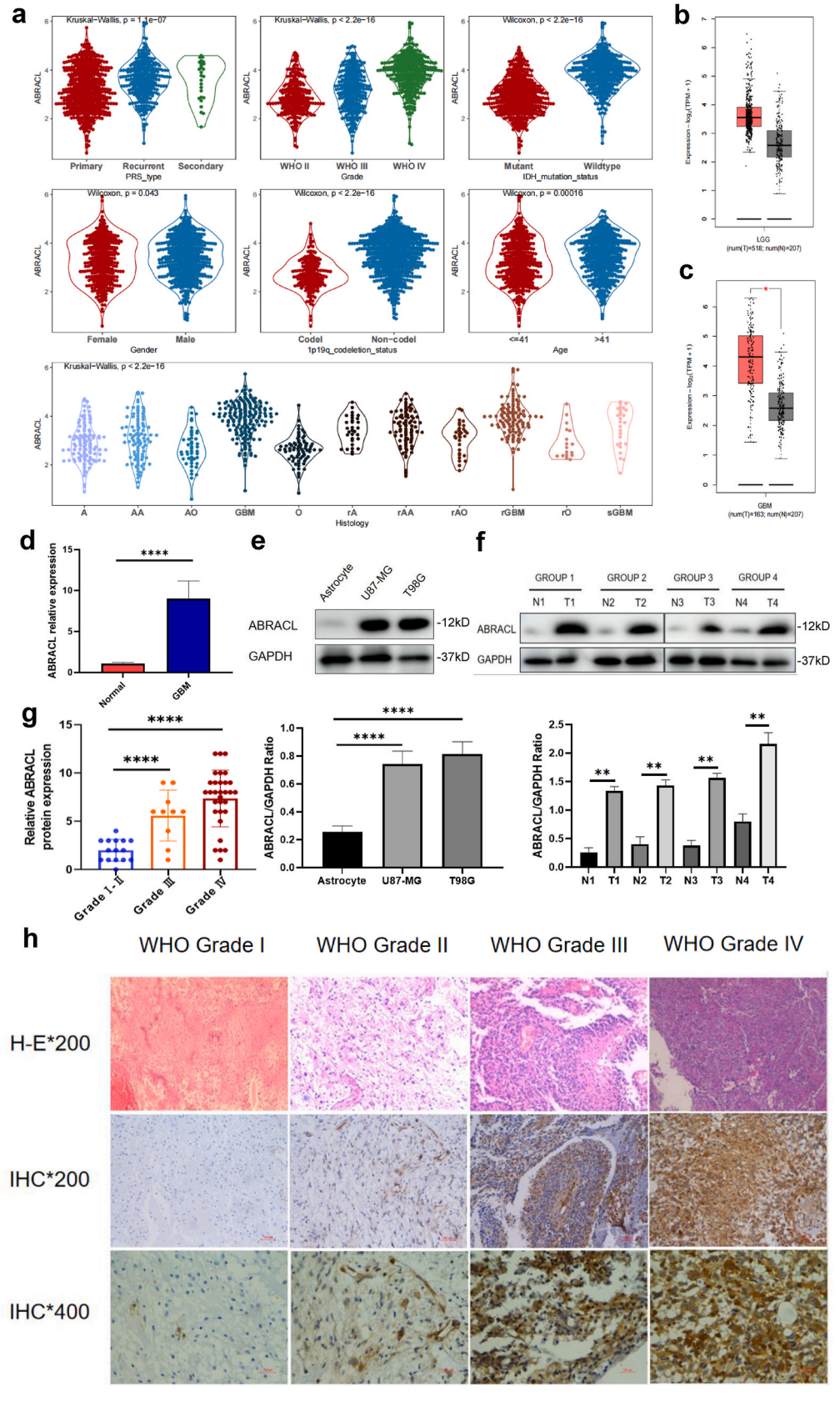

(caption on next page)

Fig. 1. The clinical value of ABRACL expression level in human glioma tissues. **a**. The violin plots show that expression level of ABRACL in the CGGA datasets based on the primary, recurrent, or secondary glioma status, tumor grade, IDH mutation status, gender, 1p/19q co-deletion status, age, and histosubtypes. **b**, **c**. The boxplots show that ABRACL mRNA expression levels in the LGG (**b**) and GBM (**c**) in the TCGA datasets. ABRACL mRNA is highly expressed in GBM in the TCGA datasets. **d**. RT-qPCR confirmed that the transcription level of ABRACL mRNA in high-grade glioma tissues of our own cohorts of glioma tissue samples was significantly higher than that in normal brain tissues ($P < 0.001$). **e**. Protein expression level of ABRACL in human astrocyte (HA cell line) and glioma cell lines (U87-MG, T98G) quantified by Western blotting ($P < 0.05$). The uncropped versions of this original western blotting image is attached in Supplement file 8. **f**. Protein expression levels of ABRACL in normal brain tissues and glioma tissues quantified by Western blotting ($P < 0.05$). The uncropped versions of this original western blotting image is attached in Supplement file 9. **g**. Hematoxylin-Eosin (200 × magnification) and immunohistochemical staining of ABRACL protein in WHO I-IV glioma tissues (200 × magnification, 400 × magnification). **h**. IRS shows that the protein level of ABRACL is highly elevated in glioma tissues with increasing WHO I-IV grades ($P < 0.001$). Codel: Co-deletion; A: astrocytoma; AA: anaplastic astrocytoma; AO: Anaplastic oligodendroglioma; GBM: glioblastoma multiforme; O: oligodendroglioma; rA: recurrent astrocytoma; rAA: recurrent anaplastic astrocytoma; rGBM: recurrent glioblastoma; rO: recurrent oligodendroglioma; sGBM: secondary glioblastoma; LGG: low grade glioma; N: normal; T: tumor; H–E: Hematoxylin-Eosin; IHC: immunohistochemical staining; IRS: immunoreactivity score. *: $P < 0.05$; **: $P < 0.01$; ***: $P < 0.001$.

Table 1
Correlation between the clinicopathological features and expression of ABRACL.

Parameters	Level	ABRACL expresssion High	ABRACL expresssion Low	*P* value
No. of patients		358	459	
PRS type (%)	Primary	190 (53.1)	319 (69.5)	<0.001
	Recurrent	152 (42.5)	129 (28.1)	
	Secondary	16 (4.5)	11 (2.4)	
Histology (%)	A	21 (5.9)	89 (19.4)	<0.001
	AA	32 (8.9)	68 (14.8)	
	AO	5 (1.4)	41 (8.9)	
	GBM	129 (36.0)	49 (10.7)	
	O	3 (0.8)	72 (15.7)	
	rA	12 (3.4)	19 (4.1)	
	rAA	44 (12.3)	42 (9.2)	
	rAO	7 (2.0)	25 (5.4)	
	rGBM	86 (24.0)	28 (6.1)	
	rO	3 (0.8)	15 (3.3)	
	sGBM	16 (4.5)	11 (2.4)	
Grade (%)	WHO II	38 (10.6)	191 (41.6)	<0.001
	WHO III	89 (24.9)	180 (39.2)	
	WHO IV	231 (64.5)	88 (19.2)	
Gender (%)	Female	142 (39.7)	198 (43.1)	0.354
	Male	216 (60.3)	261 (56.9)	
Age (mean (SD))		45.52 (13.34)	41.34 (10.88)	<0.001
OS (mean (SD))		25.12 (29.14)	57.36 (41.73)	<0.001
IDH mutation status (%)	Mutant	90 (25.1)	363 (79.1)	<0.001
	Wildtype	268 (74.9)	96 (20.9)	
1p19q codeletion status (%)	Codel	14 (3.9)	161 (35.1)	<0.001
	Non-codel	344 (96.1)	298 (64.9)	
ABRACL (mean (SD))		4.16 (0.42)	2.72 (0.55)	<0.001

PRS: primary, recurrent, or secondary; SD: standard deviation; A: astrocytoma; AA: anaplastic astrocytoma; AO: Anaplastic oligodendroglioma; GBM: glioblastoma multiforme; O: oligodendroglioma; rA: recurrent astrocytoma; rAA: recurrent anaplastic astrocytoma; rGBM: recurrent glioblastoma; rO: recurrent oligodendroglioma; sGBM: secondary glioblastoma; Codel: 1p/19q co-deletion.

2.8. DNA synthesis assay

KFluor488 click-iT EdU (KeyGen Biotech, Jiangsu, China) was used to determine the effect of ABRACL on the proliferation of glioma cells. Five thousand U87-MG and T98G cells in each group were inoculated in a 96-well plate for EDU staining. EDU labeling, cell fixation, osmosis promotion, Apollo staining and Hoechst 33342 restaining were performed according to the manufacture's protocols. Fluorescence microscopy was used to collect images and calculate EDU positive rate (the number of EDU positive cells in 3 random fields of view is divided by the number of cell nuclei in the same fields of view).

2.9. Migration and invasion assays

The migration and invasion capabilities of stable cells were detected by transwell chamber. For the migration assay, the insert in the upper chamber had pores of an 8.0 mm in diameter was placed in each well of 24-well plate transwell system. In the invasion assay, the upper chamber was pre-coated with Matrigel (Matrigel substrate: serum-free medium = 1:4, Nuova Pharmaceutical Technology, Shanghai, China). The upper chamber was placed in each well of 24-well plate as the lower chamber, and the rest of preparation steps were the same as the migration assay. For cell seeding, the stable cells (U87-MG or T98G cells) at logarithmic growth phase were

Table 2
Association of ABRACL expression level with clinicopathological parameters of glioma patients.

Parameters	No. of patients	ABRACL expression level			
		Low (n, %)	High (n, %)	Chi-square value	*P* value
WHO grade				13.73	0.004
I	1	1(100)	0(0)		
II	14	10 (71.43)	4(28.57)		
III	10	3(30)	7(70)		
IV	31	6(19.35)	25(80.65)		
Gender				0.159	0.689
Male	26	10(38.16)	16(61.))		
Female	30	10(33.33)	20(66.67)		
Age (years)				2.70	0.100
≤60	31	14(45.16)	17(54.84)		
>60	25	6(24.00)	19(76.00)		
Location				1.368	0.242
Supratentorial	39	12(30.77)	27(69.23)		
Subtentorial	17	8(47.06)	9(52.94)		
Tumor size (cm)				0.082	0.773
≤5	35	13(37.14)	22(62.86)		
>5	21	7(33.33)	14(66.67)		
KPS score				1.779	0.182
≤90	29	9(31.03)	20(68.96)		
>90	27	11(40.74)	16(59.25)		

KPS: Karnofsky Performance Status Scale.

digested with 0.25 % trypsin-EDTA, collected by centrifugation, and washed twice with PBS, and dispensed at the number of 2.5×10^4 (U87-MG) or 2.5×10^4 (T98G) cells into each well with 150 ml of serum-free DMEM medium. For the cells that were inoculated into the upper chamber of transwell system, 650 ml of DMEM complete medium were added to the lower chamber. After incubation for 24 h, the upper chamber was taken out. The cells that have not yet invaded or migrated through the barrier membrane were removed by gently wiping the interior with a cotton swab, then the bottom of the upper chamber was fixed in 4 % paraformaldehyde for 30 min, and stained with 0.1 % crystal violet for 30 min. The cells on the bottom of the upper chamber were observed under microscope. 5 fields of view at a high magnification were randomly selected and imaged. The total number of cells on the bottom of the upper chamber was counted.

2.10. Cell cycle assay

Cell cycle was detected using a Cell Cycle Detection kit (KeyGen Biotech, Jiangsu, China). After 24 h of culture, cells were digested and collected centrifugation. The cells were mixed with 250 μl of pre-cooled PBS, then slowly dropped into 750 μl of anhydrous ethanol and fixed overnight at −20 °C. After fixation, cells were centrifuged at 2000 rpm/min for 5 min, the supernatant was discarded, and the cells were re-suspended with PBS. 10 ng of RNA enzyme were added to the re-suspended cells, followed by centrifugation at 2000 rpm/min for 5 min and removal of the supernatant. After 5 μl of PI staining solution and 95 μl of 1 × analysis buffer solution were mixed well, then they were added to the re-suspended cells and allowed to incubate for 30 min without light. Cell cycle analysis was performed by flow cytometry.

2.11. Detection of apoptosis by flow cytometry (annexin-V/PI method)

Apoptosis rate of U87-MG and T98G cells was detected using an Annexin-V/PI kit (KeyGen Biotech, Jiangsu, China). Cells were cultured in 6-well plate for 24 h before harvesting. 1×10^6 cells in each group (vector control, negative control, ABRACL overexpression, and ABRACL knockdown) were re-suspended with 500 ml of 1 × binding buffer, stained with 5 ml of Annexin V-FITC and 5 ml of propidium iodide (PI) for 15 min, and gently mixed and then incubated at room temperature in the dark for 15 min. Flow cytometry was used to detect early and late apoptotic cells. Apoptosis rate was analyzed by FlowJo v10 software (BD Biosciences, CA, USA).

2.12. Rhodamine-phalloidin staining of F-actin

The stably transfected cells in each group were cultured in a chamber slide. After 24 h, the original culture medium was discarded and the cells were rinsed twice with 1 × PBS, then 200 ml of 4 % paraformaldehyde were added for fixation at room temperature for 20 min. After fixation, paraformaldehyde solution was replaced with 1x PBS rinse for 3 times, then 200 ml of 0.1 % Triton X-100 penetrating solution were added to permeablize the cell membrane for 5 min at room temperature. The lysate was aspirated and the cells were washed with PBS for 3 times. After PBS was aspirated, 200 ml of newly prepared tetramethylrhodamine (TRITC)-Phalloidin (Catalog number: 40734ES75, YEASEN Biotech Co., Ltd., China) was added to stain the washed cells in the chamber slide at room temperature in dark for 80 min, then DAPI solution (Beyotime Institute of Biotechnology, China) was added to stain cell nucleus for 5

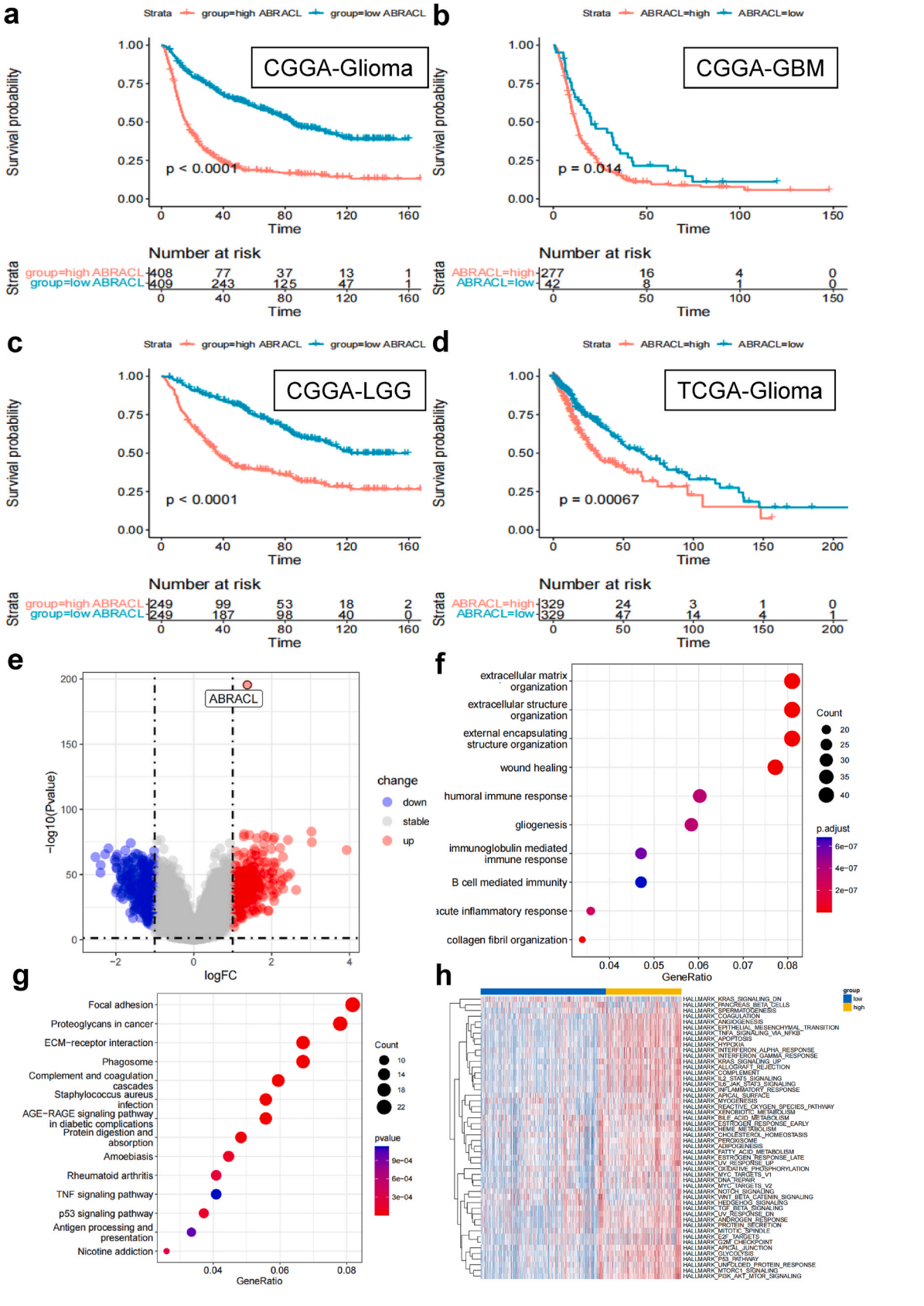

(caption on next page)

Fig. 2. The relationship between ABRACL expression and survival for glioma, and functional enrichment analysis between the ABRACL high- and low-expression groups in gliomas. **a**, **b**, **c**, **d**. Kaplan-Meier survival curves were used to analyze the overall survival of glioma patients with high expression of ABRACL and low expression of ABRACL in the CGGA and TCGA glioma datasets ($P < 0.001$). **e**. Differential expression genes (DEGs) between the groups with ABRACL low and high expression levels in TCGA glioma dataset. **f**, **g**. GO and KEGG enrichment analysis of DEGs between the ABRACL high- and low-expression groups in TCGA glioma dataset. **h**. Hallmark pathways analysis of ABRACL low-expression and high-expression groups in TCGA glioma dataset.

min. Slides were sealed with anti-fluorescent quenching sealing agent, and then examined under an orthofluorescence microscope.

2.13. RNA sequencing and determination of differential gene enrichment

Stable lentivirus transfected U87-MG cells were cultured for 24 h, then lyzed in TRIzol reagent (Catalog number: 15596026, ThermoFisher Scientific, USA), which were prepared for RNA sequencing by Novogene Technology Co., Ltd. (Beijing, China). RNA integrity was assessed using the RNA Nano 6000 Assay Kit of the BioAnalyzer 2100 system (Agilent Technologies, CA, USA). NEB libraries were built for transcriptome sequencing. GO and KEGG pathway analyses were implemented by the ClusterProfiler R package.

2.14. Nude mouse GBM xenograft model

All the animals were acclimated under standard laboratory conditions (ventilated room, 25 ± 1 °C, 60 ± 5 % humidity, 12 h light/dark cycle), and housed in plastic cages, maximum 5 mice per cage. They had free access to standard water and food. All procedures were conducted in accordance with the international guidelines on the ethical use of laboratory animals and were approved by by the Ethics Committee of the First Affiliated Hospital of Wannan Medical College (Approval number: LLSC-2022-189). The accreditation number of the laboratory is CERTIFICATE No.: 124003700348234 promulgated by Nanjing Jicui Yaokang Experimental Animal Technology Co., Ltd. Xenograft model in 10 female and 11 male BALB/c nude mice was formulated by intracranial injection of 10 ml of exponentially growing lentivirus-infected U87-MG cell suspensions at a density of 1×10^6 cell/ml (7 animals per experimental group). The mice were then observed daily for neurological symptoms, signs, mental performance, motor behavior, dietary activity, weight change, and survival time. Bioluminescent imaging was applied by giving D-Luciferin, Sodium Salt (Yeasen, Shanghai, China) via intraperitoneal injection at a luciferin/body weight concentration of 150 mg/kg. Different time points were selected to observe the formation of tumor, fluorescence intensity and other growth conditions in the brain of the mice under a Live Image System (Guangzhou Biolight Biotechnology Co., Ltd., China). After the last bioluminescent imaging or when an animal exhibited cachexia symptoms, mice were sacrificed under deep anesthesia, and the tumor tissues were removed for MMP-2 and Ki-67 immunohistochemical staining.

2.15. Statistical analysis

The R (version 4.0.2) was used for all data analysis. Survival analysis was performed using R packages, “survminer” and “survival”. A log-rank test Kaplan–Meier (KM) curve was applied to evaluate the survival divergence of different groups. The difference between the two groups was analyzed using the Wilcoxon test. The Kruskal-Wallis test was used for differential analysis among the three or more groups.Three independent experiments were performed, and the results were shown as mean ± the standard deviation (SD). GraphPad Prism 7 was used for graphing. Statistical differences between two groups were analyzed by the student’s *t*-test. One-way analysis of variance (ANOVA) was used for the comparison among three or more groups. The potential associations between ABRACL expression and clinicopathological characteristics were evaluated by chi-square test. The difference was considered as statistically significant with $P < 0.05$.

3. Results

3.1. ABRACL is highly expressed in different sub-types of gliomas

First of all, we examined the expression level of ABRACL using the public datasets of glioma in CGGA. The upregulated expression levels of ABRACL were discovered in different subtypes of gliomas in the CGGA datasets. (1) The status of primary, recurrent, or secondary glioma: the difference of ABRACL expression levels between primary and recurrent/secondary gliomas is statistically significant ($P < 0.001$, the left panel of the top panels in Fig. 1a). (2) WHO grade: The expression level of ABRACL was positively correlated to the tumor grades. Compared with WHO II glioma, the expression levels of ABRACL in grade III and IV glioma were significantly higher ($P < 0.01$, the middle panel of the top panels in Fig. 1a); and the expression level of ABRACL in grade IV glioma was higher than WHO III ($P < 0.01$, the middle panel of the top panels in Fig. 1a). (3) IDH mutation status: the mRNA level of ABRACL in the IDH wild-type group was significantly upregulated than that in the IDH mutant-type group ($P < 0.001$, the right panel of the top panels in Fig. 1a). (4) 1p/19q co-deletion status: ABRACL expression in the 1p/19q co-deletion group was higher than that in the non-deletion group ($P < 0.001$, the middle panel of the middle panels in Fig. 1a). A gender difference in terms of ABRACL expression level was noted between male and female glioma patients ($P = 0.043$, the left panel of the middle panels in Fig. 1a). An age difference with regard to ABRACL expression level existed between age greater than 41 years old patients and equal to or less than 41 years old patients ($P = 0.00016$, the right panel of the middle panels in Fig. 1a). The difference of ABRACL expression levels among different glioma

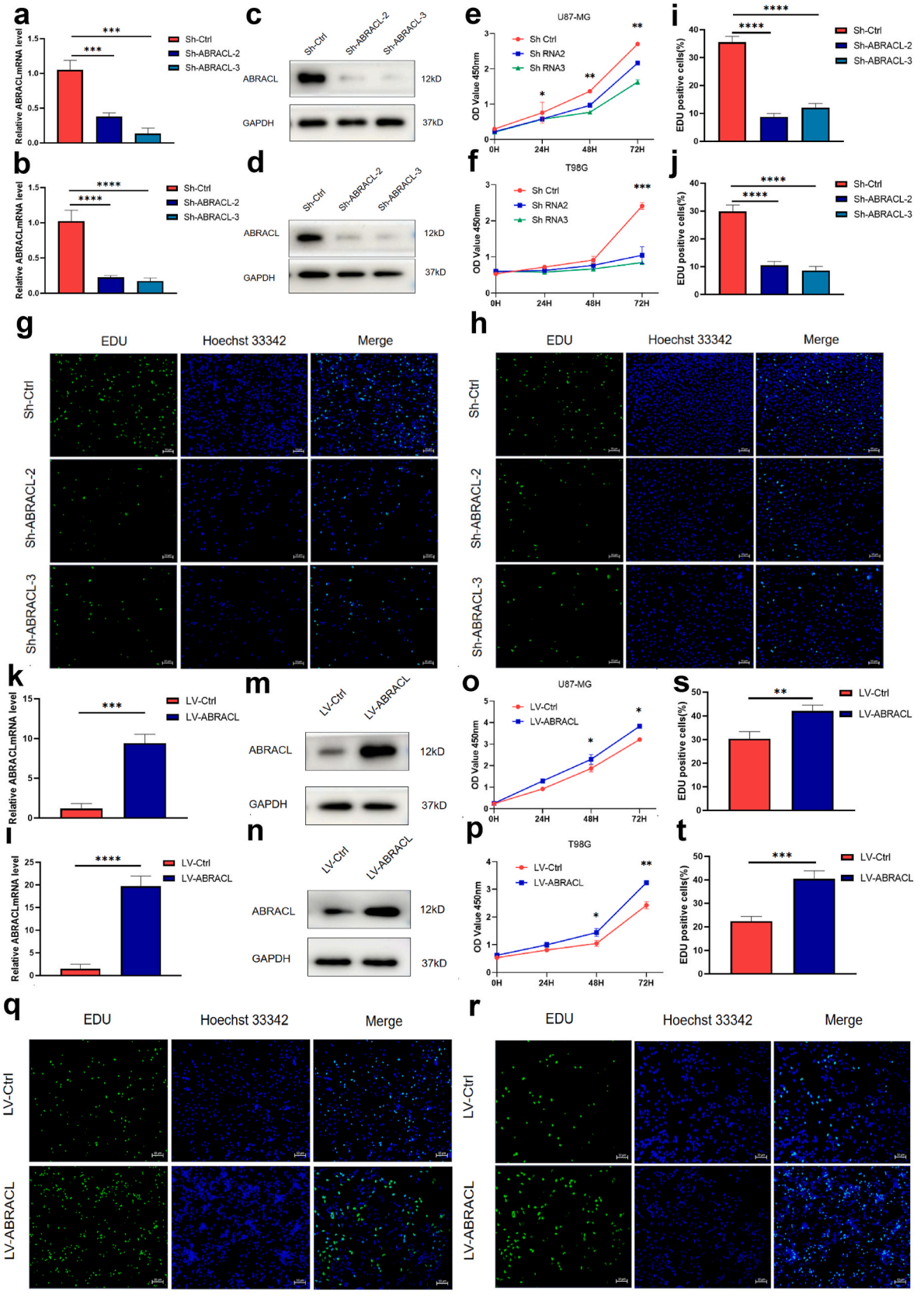

(caption on next page)

Fig. 3. ABRACL overexpression promotes the proliferation of glioma cells. **a**, **b**. RT-PCR results showing the transfection efficiency of lentiviral knockdown (Sh-ABRACL-2, Sh-ABRACL-3) in U87-MG (**a**) and T98G (**b**) glioma cell lines. **c**, **d**. Western blot results validating the transfection efficiency of sh-ABRACL-2 and sh-ABRACL-3 in U87-MG (**c**) and T98G (**d**) glioma cell lines. The uncropped versions of this original western blotting image is attached in Supplement file 10. **e**, **f**. CCK-8 results showing the proliferation of U87-MG and T98G glioma cells in response to ABRACL knockdown. **g**, **h**, **i**, **j**. EDU assays revealing ABRACL knockdown inhibits proliferation of U87-MG and T98G glioma cells. **k**, **l**. RT-PCR results identifying the transfection efficiency of lentiviral overexpression vector (LV-ABRACL) in U87-MG, and T98G glioma cell lines. **m**, **n**. Western blot results showing the transfection efficiency of lentiviral overexpression vector (LV-ABRACL) in U87MG and T98G glioma cell lines. The uncropped versions of this original western blotting image is attached in Supplement file 11. **o**, **p**. CCK-8 results showing the proliferation of U87-MG and T98G glioma cells after ABRACL overexpression. **q**, **r**, **s**, **t**. EDU assays revealing elevated ABRACL expression promoting the proliferation of U87-MG and T98G glioma cells (*P < 0.05, **P < 0.01, ***P < 0.001, ****P < 0.0001).

histosubtypes was statistically significant (P < 0.01) (the bottom panel in Fig. 1a–Table 1).

We then examined the expression level of ABRACL using another public datasets of glioma in TCGA. Although no significant difference was found for ABRACL mRNA expression levels between low grade glioma and normal tissues, WHO IV gliomas still exhibited significantly higher ABRACL mRNA level (P < 0.05, Fig. 1b and c).

In order to validate whether the differentially upregulated expression level of ABRACL in glioma of different WHO grades found in the CGGA and TCGA datasets, compared with the normal tissues, we performed RT-qPCR using the total RNA extracted from our cohort of human surgical glioma samples (GBM specimen). RT-qPCR data validated that ABRACL was significantly upregulated in the tissues from glioblastoma patients compared to the normal brain tissues (P < 0.001) (Fig. 1d). Western blotting analysis revealed that the ABRACL protein level in U87-MG and T98G glioblastoma cell lines were higher than human astrocyte cell line (HA) (Fig. 1e). And subsequent Western blot also showed the expression level of ABRACL in GBM tissues was significantly higher than the normal tissues (Fig. 1f). Hematoxylin-eosin staining was performed on tissue sections from glioma patients to confirm the pathological diagnosis before we performed the IHC staining using these same tissues (Fig. 1h, top panels). The IHC results showed that ABRACL protein expression levels in glioma tissues were gradually increased along with the increasing WHO grades in glioma tissues (Grade I-II: 2.000 ± 0.2298; Grade III: 5.6 ± 0.8327; Grade IV: 7.371 ± 0.5277, P < 0.05) (middle and bottom panels of Fig. 1g; Fig. 1h). IHC H-scores of WHO grades III and IV were significantly increased, compared to low-grade glioma, and the difference was statistically significant (P < 0.05) (Fig. 1h–Table 2).

3.2. High level of ABRACL is associated with poor prognosis in glioma patients

Glioma patients were divided into ABRACL high and low expression level groups, according to the median level of ABRACL expression. The survival analysis of glioma patients in CGGA glioma datasets showed that the overall survival (OS) (P < 0.0001, Fig. 2a) of patients in the ABRACL high expression level group were significantly shorter than those in the low expression level group. The OS in high ABRACL expression level group was significantly shorter than that in low expression level group in CGGA-GBM dataset (P = 0.014, Fig. 2b); The OS in ABRACL high expression level group was worse than that in low expression level group in CGGA-LGG datasets (P < 0.0001, Fig. 2c) and TCGA-Glioma dataset (P < 0.00067, Fig. 2d). In short, the high expression level of ABRACL is closely related to the poor prognosis of patients with glioma. Then, we analyzed DEGs between the groups with ABRACL low and high expression levels in TCGA glioma datasets. We confirmed that ABRACL gene was one of the DEGs. In fact, ABRACL was the most upregulated gene among all DEGs (Fig. 2e).

To find the ABRACL's biological functions and involvement in biological processes, GO enrichment analysis for biological functions and KEGG enrichment analysis were performed. The results of GO enrichment analysis indicate that high ABRACL expression may mainly correlate with extracellular matrix and structure organization, external encapsulating structure organization and wound healing (Fig. 2f). The results of KEGG enrichment analysis show that ABRACL expression may be associated with biological processes and signaling pathways, such as focal adhesion, extracellular matrix receptor interaction, and p53 signaling pathway (Fig. 2g). Furthermore, GSEA analysis prompted that K-RAS signaling, TNF-α, IL-2/STAT5, JAK/STAT3 signaling pathways may participate in the regulation of ABRACL (Fig. 2h). In addition, the analysis of a set of marker genes for tumor-infiltrating immune cells indicated that many different types of immune cells including activated B cells, activated CD4 T cells, regulatory T cells, activated dendritic cells and natural killer cells occupied higher percentages of infiltrating immune cells in glioma microenvironment (Fig. S1).

3.3. ABRACL overexpression promotes the proliferation of glioma cells

Each of two independent lentiviral vector-based shRNA constructs was used to knock down ABRACL expression in U87-MG and T98G glioma cells. RT-qPCR and Western blotting validated that ABRACL expression level was significantly knocked down in U87-MG and T98G glioma cells (Fig. 3a–d). CCK-8 assay was carried out to investigate the proliferation rate of U87-MG and T98G cells in Sh-ABRACL group (Sh-RNA2, Sh-RNA3) and the Sh-scrambled control group (Sh-Ctrl). The results demonstrated that knockdown of ABRACL expression level inhibited cell proliferation rate of U87-MG and T98G cells (Fig. 3e and f). We also performed EDU assays to examine the effect of ABRACL on cell proliferation of U87-MG and T98G whose ABRACL was knocked down. The results discovered that the percentage of EDU-positive cells (green in color) in Sh-ABRACL cells was significantly lower than that of control group (Fig. 3g and h). Quantitative analysis of the EDU assay indicated that ABRACL knockdown resulted in a statistically significant decrease of EDU-positive cells in both U87MG and T98G cells (Fig. 3i and j; P < 0.01 and P < 0.01, respectively). To further confirm the function of ABRACL in cell proliferation, we performed overexpression of ABRACL in U87-MG and T98G cells. RT-qPCR showed that ABRACL was

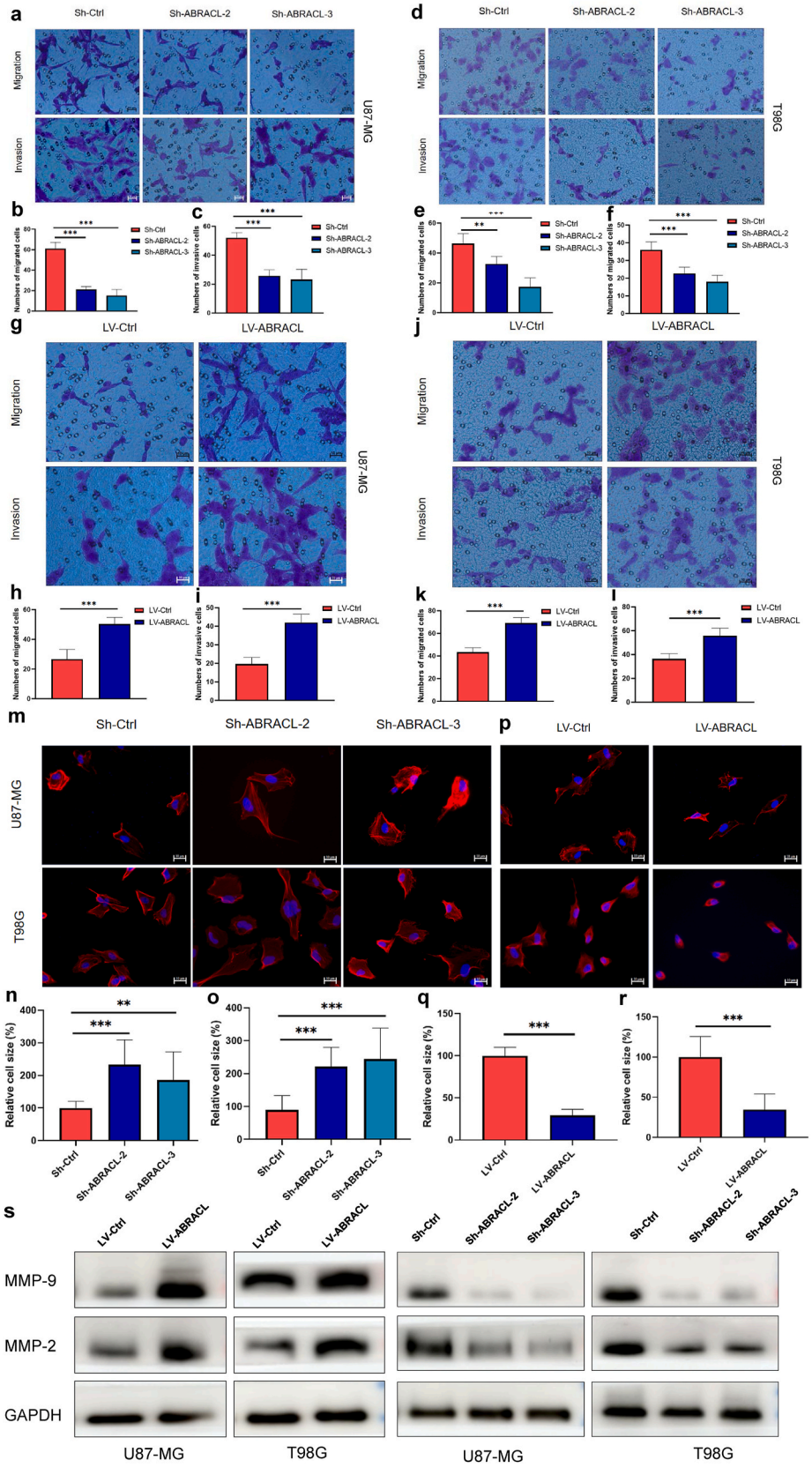

(caption on next page)

Fig. 4. ABRACL overexpression promotes the migration, invasion and cytoskeletal transition of glioma cells. **a**, **b**, **c**. The migration ability examined by transwell migration assay and the statistical histogram of the quantification of migrated cells after ABRACL knockdown in U87-MG glioma cells in response to ABRACL knockdown. **d**, **e**, **f**. The migration ability examined by transwell migration assay and the statistical histogram of the quantification of migrated cells after ABRACL knockdown in T98G glioma cells in response to ABRACL knockdown. **g**, **h**, **i**. The migration ability examined by transwell migration assay and the statistical histogram of the quantification of migrated U87-MG cells in response to overexpression of ABRACL. **j**, **k**, **l**. The migration ability examined by transwell migration assay and the statistical histogram of the quantification of migrated T98G cells in response to overexpression of ABRACL. **m**, **n**, **o**. Rhodamine-phalloidin staining shows that the morphology of U87-MG and T98G ABRACL knockdown cells changed significantly and became longer, and the cell size became larger. **p**, **q**, **r**. Overexpression of ABRACL making the cell morphology become shorter and the cell size become smaller in up-regulated U87-MG and T98G ABRACL cells. **s**. Western blot analysis exhibiting MMP-2 and MMP-9 were highly expressed in ABRACL overexpression (LV-ABRACL) group in both U87MG and T98G glioma cells, and ABRACL knockdown cells displayed decreased MMP-2 and MMP-9 protein levels (*$P < 0.05$, **$P < 0.01$, ***$P < 0.001$, ****$P < 0.0001$). The uncropped versions of this original western blotting image is attached in Supplement file 12 and Supplement file 13.

significantly overexpressed in U87-MG and T98G cells (Fig. 3k and l), and Western blotting further validated that ABRACL was overexpressed (Fig. 3m and n). CCK-8 assays showed that overexpression of ABRACL enhanced cell proliferation of U87-MG and T98G cells (Fig. 3o and p). EDU staining results showed that the percentage of green cells in LV-ABRACL group was obviously higher than LV-Ctrl group (Fig. 3q and r). Overexpression of ABRACL exhibited a statistically significant increase of EDU-positive cells in both U87-MG and T98G cells (Fig. 3s and t; $P < 0.01$ and $P < 0.01$, respectively). These results indicated that ABRACL promotes glioma cell proliferation in U87-MG and T98G glioma cells.

3.4. ABRACL overexpression promotes the migration, invasion and cytoskeleton of glioma cells

As the most aggressive malignant brain tumor, glioma cells possess a strong and aggressive ability of migration and invasion. Given the relationship between elevated expression of ABRACL and poor prognosis as one of the clinicopathological features of glioma patients, ABRACL was considered to play a role in the invasion and migration of glioma cells. To confirm whether ABRACL affects the cytodynamics of glioma cells, we used transwell and Matrigel to further evaluate the roles of ABRACL in migration and invasion of U87-MG and T98G glioma cells. The results showed that the number of invasive and migrated cells transfected with Sh-ABRACL was significantly decreased, compared with the control group (Fig. 4a–f; $P < 0.01$), and over-expression of ABRACL significantly facilitated the number of invasive and migrated U87-MG and T98G glioma cells (Fig. 4g–l; $P < 0.01$), suggesting that knockdown of ABRACL contributes to inhibiting the invasive and migration ability of U87-MG and T98G glioma cells. Next, we sought to examine whether ABRACL affects cytoskeletal dynamics using Rhodamine-phalloidin staining. We observed the effect of ABRACL knockdown on cytoskeleton and cell morphology through Rhodamine-labeled phalloidin. It was found that compared with the control group, the morphology of ABRACL knockdown cells was changed significantly and became longer, and the cell size became larger (Fig. 4m, n, o; $P < 0.01$). However, overexpression of ABRACL displayed the opposite changes (Fig. 4p, q, r; $P < 0.01$). In order to further elucidate the molecular mechanism of cytoskeletal changes observed, we examined the expression levels of MMP-2 and MMP-9 proteins in cells of each group. Western blot analysis results exhibited that MMP-2 and MMP-9 were highly expressed in LV-ABRACL group in both U87-MG and T98G glioma cells, compared with control group (Fig. 4s, left two panels). In contrast, ABRACL knockdown cells exhibited decreased levels of MMP-2 and MMP-9 protein (Fig. 4s, right two panels). These results reveal that ABRACL overexpression promotes the migration, invasion and cytoskeletal dynamics of glioma cells.

3.5. ABRACL overexpression facilitates cell cycle arrest and inhibits cell apoptosis in human glioma cells

We further investigated the effect of ABRACL on cell cycle by flow cytometry. ABRACL knockdown led to cell cycle arrest in the G1 phase (Fig. 5a, b, c) and ABRACL over-expressing cells displayed decreased the population of the U87MG and T98G cells in the G1 phase by 4.8 % and 9.41 %, respectively (Fig. 5d, e, f). Furthermore, cells of ABRACL knockdown group showed a higher percentage of apoptotic events, compared with cells in control group in both U87-MG and T98G cells lines (Fig. 5h and i; $P < 0.01$). In contrast, ABRACL over-expressing cells appeared a higher percentage of survival cells, compared with cells of control group in both U87-MG and T98G cells lines (Fig. 5g–j; $P < 0.01$). Thereafter, we explored some of the key known proteins involved in the apoptosis process in glioma cells. Western blot results indicated that Bcl-2, an anti-apoptotic protein, was remarkably increased in both ABRACL over-expressing U87-MG and T98G cells, accompanied with a decreased level of Bax, a pro-apoptotic protein (Fig. 5k, left two panels). In contrast, ABRACL knockdown inhibited Bcl-2 expression level and increased Bax protein level (Fig. 5k, right two panels). These results demonstrate that ABRACL facilitates cycle arrest and inhibits cell apoptosis in U87-MG and T98G glioma cells.

3.6. Overexpression of ABRACL enhances the activity of STAT3 signaling pathway

STAT3 signaling pathway is important for the regulation of gliomagenesis and aggressiveness [10]. However, whether ABRACL promotes the malignant phenotype of glioma cells by affecting STAT3 signaling pathway remains unclear. To further explore the mechanism of ABRACL's effects against GBM, total RNA was extracted from U87-MG cells with ABRACL overexpression or knockdown, and then were used for RNA sequencing (RNA-seq). The RNA-seq results revealed 1293 up-regulated and 793 down-regulated genes in U87-MG cells with ABRACL overexpression, compared to control cells (differential regulation was defined as fold change >2 and $P < 0.05$, Fig. 6a). In contrast, the sh-ABRACL group had 857 differentially up-regulated genes and 534 downregulated genes

(Fig. 6c). The Venn diagram intersection of each group revealed 266 DEGs in common (Fig. 6b). GO analysis found that the DEGs enriched were involved in the regulation of actin cytoskeleton, cytokine-cytokine receptor interaction and JAK/STAT signaling pathway (Fig. 7e and f). Furthermore, Western blotting was performed to detect the key known proteins that are involved in the STAT3 signaling pathway. Our results revealed that ABRACL overexpression in U87-MG and T98G glioma cells markedly increased the level of phosphorylated STAT3 (Fig. 6g, left two panels). However, phosphorylated STAT3 was significantly decreased in ABRACL knockdown U87-MG and T98G glioma cells, whereas total STAT3 levels did not change significantly in U87-MG and T98G glioma cells (Fig. 6g,

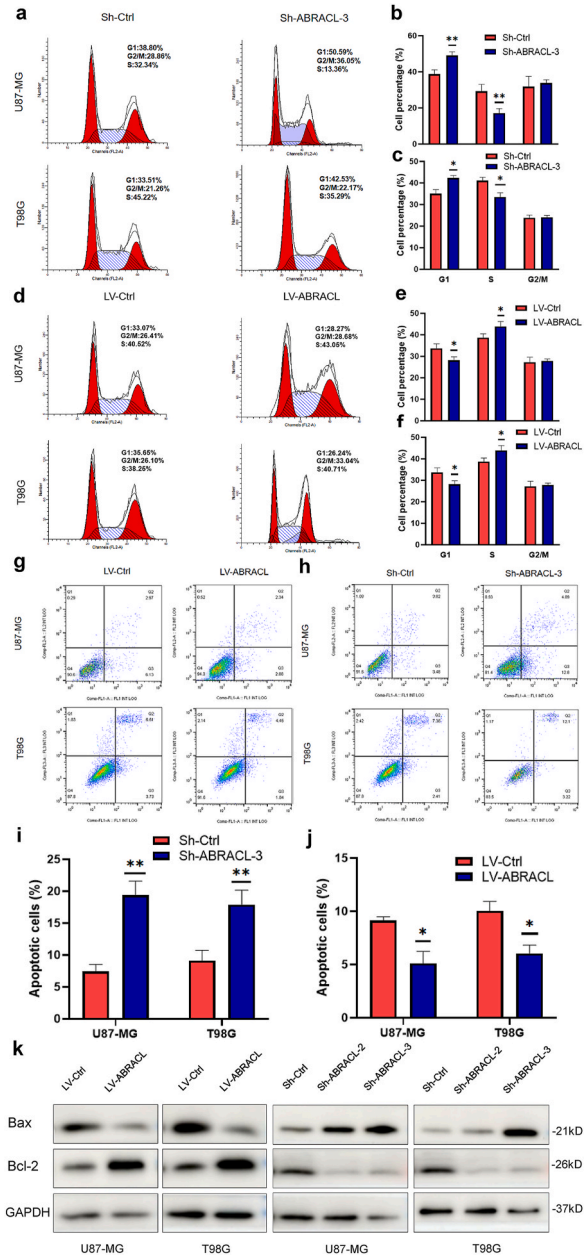

Fig. 5. ABRACL knockdown blocks cell cycle and promotes cell apoptosis in human glioma cells. **a**, **b**, **c**. Cell cycle profiles determined from Propidium iodide (PI) staining in flow cytometry demonstrating ABRACL knockdown (Sh-ABRACL) leads to cell cycle arrest in the G1 phase in the U87-MG and T98G cells. **d**, **e**, **f**. ABRACL over-expression decreases the cell population of the U87-MG and T98G cells in the G0 phase. **g**, **h**, **i**, **j**. Cell apoptotic rate was enhanced in ABRACL knockdown group, while ABRACL overexpression inhibited cell apoptosis. **k**. Key apoptosis-related proteins (Bax, Bcl-2) in U87-MG and T98G cells with ABRACL overexpression or knockdown were investigated by Western blot analysis (*P < 0.05, **P < 0.01, ***P < 0.001, ****P < 0.0001). The uncropped versions of this original western blotting image is attached in Supplement file 14 and Supplement file 15. LV-Ctrl: positive control group; LV-ABRACL: ABRACL over-expression group; Sh-Ctrl: negative control group; Sh-ABRACL: ABRACL knockdown group.

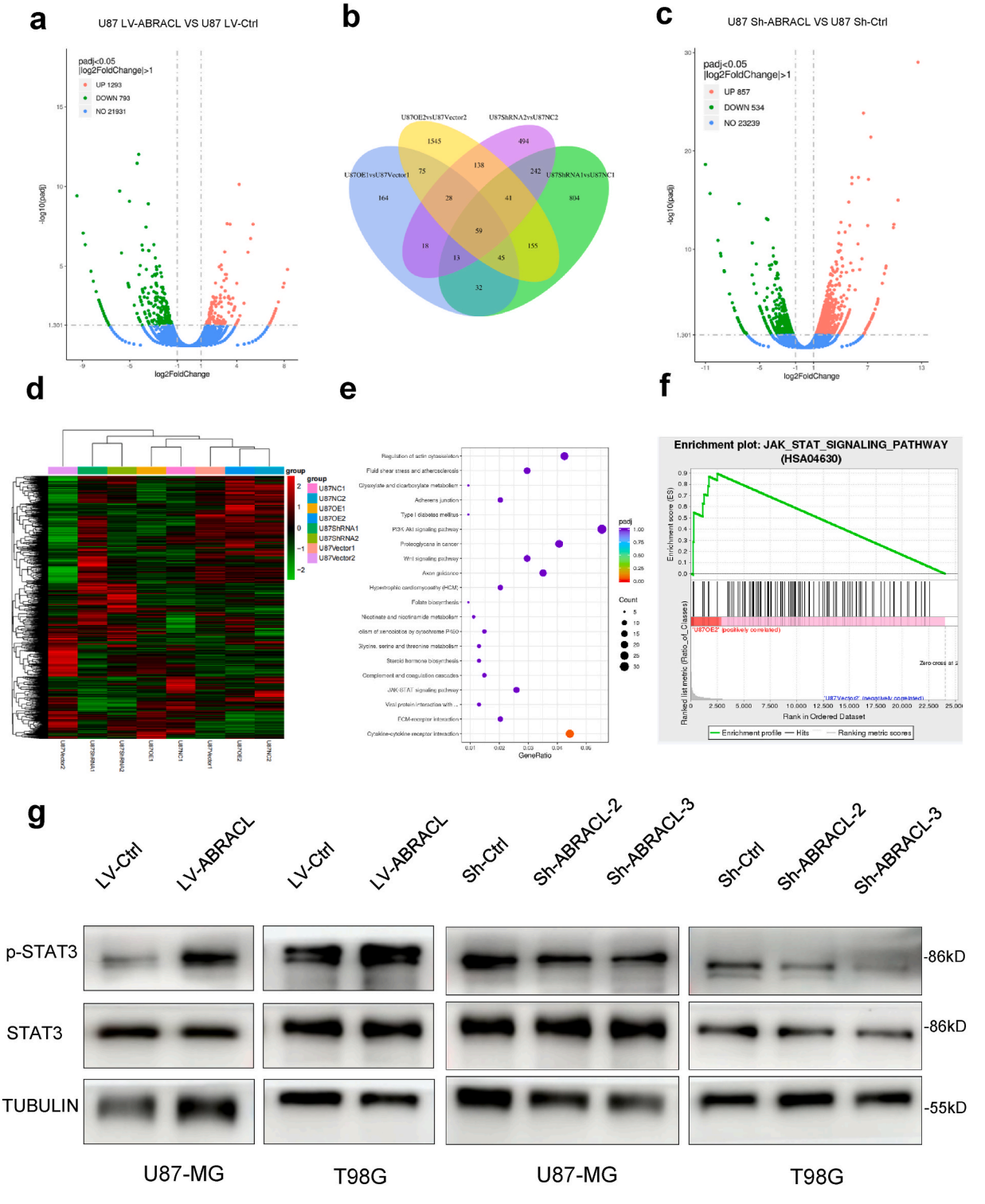

(caption on next page)

Fig. 6. Overexpression of ABRACL enhances the activity of STAT3 signaling pathway. **a**, **b**, **c**, **d**. Visualization of differentially expressed genes (DEGs) by volcano plots (**a**, **c**) and Venn diagram (**b**) in U87-MG cells with overexpression (**a**) or knockdown (**c**) of ABRACL. Green points for down-regulated genes, red points for up-regulated genes, and blue points for unchanged genes. **e**, **f**. DEGs enriched according to GO analysis were involved in the regulation of actin cytoskeleton, cytokine-cytokine receptor interaction and JAK/STAT signaling pathway. **g**. Western blotting analysis showing the expression levels of ABRACL, STAT3, p-STAT3 in each indicated group of U87-MG and T98G glioma cells. The uncropped versions of this original western blotting image is attached in Supplement file 16 and Supplement file 17. LV-Ctrl: positive control group; LV-ABRACL: ABRACL over-expression group; Sh-Ctrl: negative control group; Sh-ABRACL: ABRACL knockdown group; p: phosphorylated. (For interpretation of the references to color in this figure legend, the reader is referred to the Web version of this article.)

right two panels). In order to verify the function of ABRACL through STAT3, a small molecular targeted STAT3 inhibitor, which can inhibit the binding of high affinity phosphopeptides to the SH2 domain of STAT3, stattic [21] was used on U87-MG and T98G ABRACL overexpressed cell lines. The detected half maximal inhibitory concentration (IC50) of stattic on U87-MG and T98G ABRACL over-expressed cell lines is 4.23 μM and 5.442 μM, respectively (Fig. 7a and b). Cell proliferation assay showed that 5 μM stattic can significantly supress the growth of U87-MG and T98G ABRACAL overexpressed cell lines, compared with the control groups (Fig. 7c and d; $P < 0.001$). In addition, transwell migration and invasion assays also demonstrated that stattic can effectively inhibit the migration and invasion ability of U87-MG and T98G ABRACL overexpressed cell lines, compared with the control group (Fig. 7e–i; $P < 0.001$). These results imply that ABRACL regulates STAT3 pathway which is important for the aggressiveness of U87-MG and T98G cells. Combined with our other results in this study, we can deduce that ABRACL might increase the aggressiveness of glioma cells by affecting the STAT3 signaling pathway.

3.7. ABRACL silencing impairs the invasiveness of GBM cells and suppresses tumor growth in vivo

To further estimate the role of ABRACL in glioma cell self-renewal and tumor formation, the intracranial xenograft mouse model was established using U87-MG cells (Fig. 8a). Tumors in each group were detectable by living image system at day 7, 14, 21 and 28 after intracranial xenograft (Fig. 8b). The results revealed that ABRACL knockdown significantly reduced the tumor size as evidenced by the intensity of fluorescence detected in tumors in ABRACL knockdown (Sh-ABRACL) group that grew more slowly, compared to normal control tumors (Fig. 8b). In contrast, tumors in overexpression (LV-ABRACL) group was larger than that of control tumors (Fig. 8b; $P < 0.01$). Fluorescence intensity in each group was significant different (Fig. 8c; $P < 0.01$). Kaplan-Meier survival curves indicated that tumor-bearing mice in ABRACL overexpression (LV-ABRACL) group exhibited shorter OS than the control group (Fig. 8d). However, tumor-bearing mice in ABRACL knockdown (Sh-ABRACL) group displayed significantly longer OS time than control group (Fig. 8d). Interestingly, H&E staining suggested that the tumors from in ABRACL overexpression (LV-ABRACL) group mice exhibited a remarkable invasive tumor border, compared to tumors from ABRACL knockdown (Sh-ABRACL) group (Fig. 8e). We also detected ABRACL downstream molecules by immunohistochemistry in intracranial tumors. The immunostaining results showed that MMP-2 and Ki-67 expression levels were significantly stronger than those in control group (Fig. 8e, left panels vs. middle panels), and MMP-2 and Ki-67 expression levels in sh-ABRACL group were much weaker, compared with control group (Fig. 8e, right panels vs. middle panels). Taken together, these findings reveal that ABRACL knockdown impairs tumor growth of glioma in vivo, suggesting that ABRACL might be required for tumor growth.

4. Discussion

Glioma is the most lethal and aggressive brain tumor, accounting for about 40%–50 % of intracranial neoplasms [22]. Rapid and progressive invasion is one of the main reasons for the high mortality and recurrence of glioma, even combined with radiotherapy and chemotherapy [2]. Due to the peculiarity of the intracranial location and aggressive invasiveness of glioma tumor cells, there is no obvious margin between glioma and normal brain tissues [6]. Therefore, it is difficult to achieve the goal of radical large-scale resection, especially in important brain functional areas. In order to overcome the current treatment dilemma, new therapeutic targets that regulate this malignant invasion process are actively being pursued and urgently needed.

ABRACL has been regarded as a regulator of cell motility, actin cytoskeleton and cell movement, which is closely related to migration, invasion and infiltration of several types of cancer [23], which belongs to a new family of low molecular weight proteins, with a highly conserved sequence in different species. Interestingly, ABRACL gene only exists in eukaryotes, but not in fungi. Comparing the C-terminal 80 residue domains of proteins in the family, it was found that ABRACL has a conserved hydrophobic groove, which may allow ABRACL to interact with other proteins [10]. Several recent studies have reported the expression and functions of ABRACL in different tumors, including breast cancer, gastric and colorectal cancers [16–18]. In 2020, some scholars found that the expression level of ABRACL in gastric cancer tissue was significantly higher than that in normal tissues, and the increased level of ABRACL significantly affected the overall prognostic survival of gastric cancer patients [16]. In 2016, Stylianopoulou and other scholars identified ABRACL as an atypical winged helix protein, which can interact with the members of actin-binding Rho activator protein family, controlling proliferation and differentiation of neural progenitor cells [23]. These results reflect that ABRACL is significantly associated with worse prognosis and that overexpression of ABRACL increases the infiltration of tumor cells. In the current study, we discovered that ABRACL expression level was significantly altered in the tissues from malignant glioma patients and GBM cell lines. This suggests that ABRACL likely plays a unique role in malignant glioma.

Given the assumption that ABRACL has an important role in glioma, analysis of clinicopathological characteristics of glioma samples through RT-qPCR and Western blotting as well as mRNA level data obtained from CGGA and TCGA glioma datasets implicated

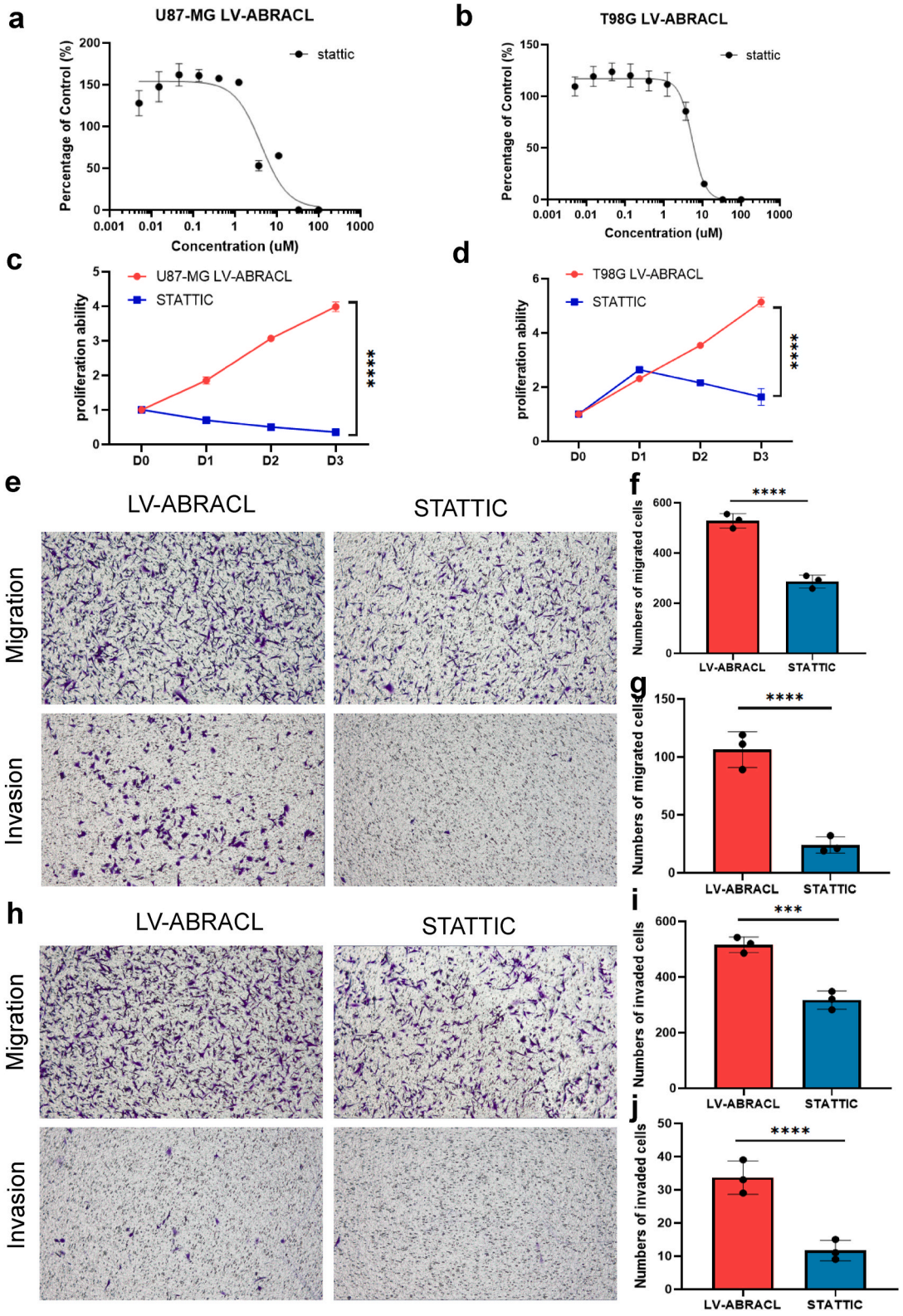

Fig. 7. Small molecular targeted STAT3 inhibitor, stattic inhibit the proliferation, migration and invasion of U87-MG and T98G ABRACL over-expressed cell lines. **a,b.** IC50 dose curve of stattic on U87-MG and T98G ABRACL overexpressed cell lines, 4.23 μM and 5.442 μM, respectively. **c,d.** Cell proliferation assay showed that 5uM stattic can significantly supress the growth of U87-MG and T98G ABRACL overexpressed cell lines,

compared with the control groups. **e,f,g.** The migration and invasion ability examined by transwell assay and the statistical histogram of the quantification of migrated and invaded U87-MG overexpression of ABRACL cells in response to 5 μM stattic. **h,i,j.** The migration and invasion ability examined by transwell assay and the statistical histogram of the quantification of migrated and invaded T98G overexpression of ABRACL cells in response to 5 μM stattic. (IC50, half maximal inhibitory concentration,*P < 0.05, **P < 0.01, ***P < 0.001, ****P < 0.0001).

that ABRACL was expressed much more highly in GBM than in normal brain tissues, which was also correlated with WHO glioma grades. Additionally, IHC results displayed that ABRACL was located in cytoplasm, and the staining intensity was increased with the increasing WHO grades, all of which suggest that ABRACL may play a role in the occurrence and development of malignant glioma. Isocitrate dehydrogenase 1 (IDH1) mutation defines a distinctly pathologically molecular subtype of diffuse glioma [24]. Glioma patients with IDH1 mutation can survive longer than patients with IDH1-wild type glioma [25]. It was found that IDH1 mutations are prevalent in about 80 % of low-grade glioma and secondary GBMs [26]. Our investigation demonstrated that ABRACL level in IDH1-WT gliomas was higher than in IDH1-Mut gliomas for each WHO grade. The present study indicates that ABRACL can be used as one of the potential biomarkers to predict the efficacy of radiotherapy and chemotherapy in GBM patients, which also indicates the prognostic value of ABRACL in glioma. This interesting implication provides us a reliable foundation for further study of ABRACL in glioma.

ABRACL is associated with biological processes in several kinds of tumors during tumorigenesis [18]. Malignant gliomas are a family of neoplastic diseases, which are characterized by higher cell proliferation, stronger motility, reduced apoptosis, and more active angiogenesis [4,27,28]. Some scholars have reported that upregulation of ABRACL could promote tumor growth and facilitate cell motility through its interaction with cofilin [18]. However, the functions of ABRACL in malignant glioma remain poorly understood so far. In this study, we demonstrated that the overexpression of ABRACL could effectively increase the proliferation of U87-MG and T98G glioma cells. Cell cycle and apoptosis play an important role in the evolution of organisms and the development of neoplasm, which reflect the progression of cell proliferation [29,30]. Our results suggested that ABRACL knockdown induced apoptosis and arrested glioma cell cycle. Consistently, Li et al. showed that ABRACL knockdown could suppress the proliferation of breast cancer MCF-7 and MDA-MB-231 cells through epithelial-mesenchymal transition [17]. In addition, our GO analyses and KEGG enrichment implicated that high ABRACL level was closely related to extracellular matrix organization and external encapsulating structure organization. A variety of investigations showed that these processes greatly contribute to tumor cell proliferation and self-renewal. These results are consistent with the data obtained from our subsequent multiple cell proliferation assays.

Glioma progression is a dynamic biological process [6]. To infiltrate firmly, tumor cells need to change cell morphology and reshape the cytoskeleton [31]. Our previous study revealed that reconstructed glioma cytodynamics plays a vital role in malignant gliomas and contributes to tumor invasion [20]. Cell migration behavior correlated to many factors such as actin polymerization-mediated protrusion and actomyosin contractility. Under complex tumor microenvironment, tumor cells trigger cytodynamics-related genes and pathways to promote cancer progression and migration [32]. Our study demonstrated that over-expression ABRACL contributed to stronger migration and invasion ability, and ABRACL knockdown inhibited glioma cell cytodynamics. Rhodamine-phalloidin staining assay showed that compared with the control group, the morphology of ABRACL knockdown cells changed significantly cumbersome, and the cell shape and cell size became elongated and larger, respectively, while ABRACL upregulation allowed cells to change their shapes markedly easily and become shorter as well to change their sizes smaller. Microfilaments are the thinnest of the three cytoskeletal structures, mainly composed of actin, and exist in the form of free spherical actin (G-actin) or F-actin. After ABRACL knockdown, the polymerization/depolymerization state of F-actin was changed, resulting in the relative decrease of F-actin, thus showing the weakening of cytoplasmic fluorescent staining and increased cell shape. A number of studies have indicated that matrix metalloproteinases (MMPs) can degrade basement membrane and extracellular matrix, and, therefore, prompting the infiltration and invasion of tumor cells [32]. Our subsequent Western blot analysis indicated ABRACL over-expression increased the expression levels of MMP2 and MMP9. This may result in an increase in the tumor's ability to degrade extracellular matrix substrates and components membrane and, thereby promoting cell progression and invasion. Consistently, Hsiao et al. discovered that ABRACL regulates the dynamics of actin by interacting with cofilin, thereby accelerating the movement of colorectal cancer cells, which in turn leads to the distant metastasis of colorectal cancer [18]. In addition, Fan et al. concluded that ABRACL affects the invasion and migration of esophageal cancer [19]. These results reflect that ABRACL may promote glioma cell migration and invasion by matrix metalloproteinases.

In order to further illustrate the underlying mechanisms by which ABRACL is involved in the tumorigenesis of glioma, we further performed GSEA. GSEA data indicated that ABRACL-associated genes were positively related to extracellular structure via JAK/STAT3 signaling. Numerous research have revealed that STAT3 transcriptionally regulates diverse downstream target genes [33,34], which play crucial roles in tumor cell growth, migration, invasion, and immune escaping [35]. Our analysis confirmed that ABRACL overexpression increased p-STAT3 protein level, while ABRACL knockdown inhibited the protein level of p-STAT3, and small molecular targeted STAT3 inbibitor stattic can significantly inhibit the proliferation, migration and invasion ability, indicating that ABRACL promotes the proliferation, migration, metastasis and cytodynamics of glioma cells by activating STAT3 signaling.

Despite these findings, this study still has certain limitations. Firstly, the upstream regulating factors (such as transcription factors, non-coding RNAs or cytokines) that may drive the activation of ABRACL in glioma are still unknown. Secondly, The direct cytodynamics and mechanisms behind cell migration and invasion should be further illustrated to explore the deeper role of ABRACL in glioma genesis and evolution.Thirdly, clinicopathological data were analyzed from 56 samples of glioma patients, which may lead to statistical bias due to the relatively small sample size. Therefore, further studies are required to clarify the implicit regulative mechanisms of ABRACL in glioma.

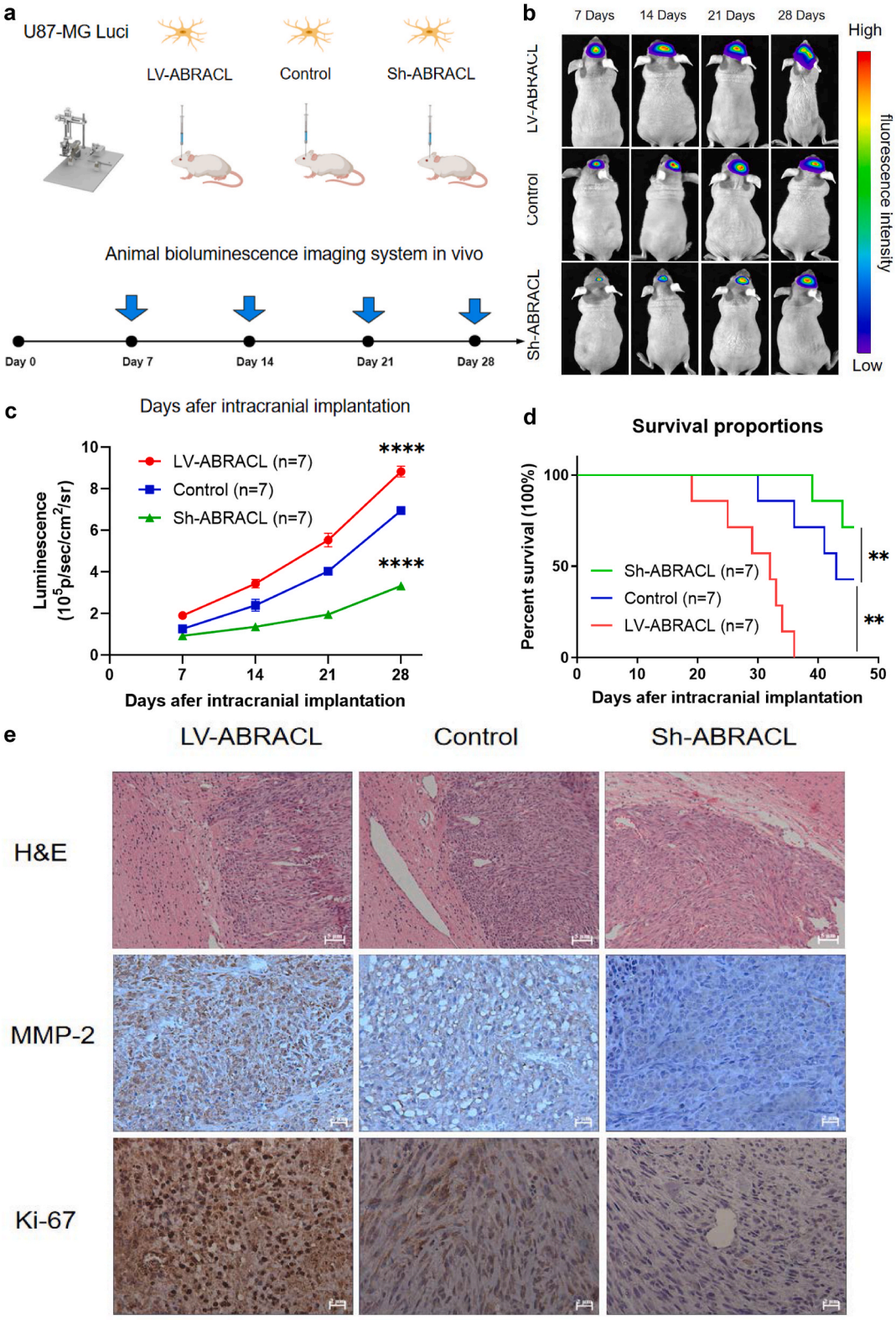

Fig. 8. ABRACL silencing inhibits tumorigenesis and impairs the invasiveness of GBM cells in vivo. **a**. Schematic diagram of experimental grouping, intracranial injection, and bioluminescence detection of the intracranial xenograft mouse model. **b**, **c**. Tumor growth and bioluminescent signals were monitored using living image system at days 7, 14, 21, and 28 after implantation. **d**. Kaplan-Meier survival curves of overall survival indicating

the percentage of survival mice in each indicated group. **e**. Representative images of H & E staining of the tumor margin and immunohistochemical staining for MMP-2 and Ki-67 in xenograft tissue sections from mice intracranially injected with U87-MG cells. Scale bar = 5 μm. LV-Ctrl: positive control group; LV-ABRACL: ABRACL over-expression group; Sh-Ctrl: negative control group; Sh-ABRACL: ABRACL knockdown group; Luci: luciferin.

5. Conclusions

In conclusion, the present work describes the molecular and clinicopathological characterizations of ABRACL in glioma. Increased ABRACL expression levels are positively associated with higher WHO glioma grades, IDH1 mutation status, and unfavorable prognosis. For the first time, we associate ABRACL with glioma cell proliferation, migration, and infiltration via STAT3 signaling, suggesting that ABRACL may represent a potential therapeutic target for glioma.

Ethics approval and consent to participate

The study protocol was approved by the Ethics Committee of the First Affiliated Hospital of Wannan Medical College. The ethical code was No. WNMC-LSD-202020. All methods were performed in accordance with the relevant guidelines and regulations. Informed consents were acquired from all study individuals for the acquisition of clinical and pathological information and the use of clinical specimens.

Data availability

The datasets used and analyzed during the current study are not publicly available due to the experimental data of this study involves the privacy of patients, which will be made available by the corresponding author. Requests to access these datasets should be directed to Xiaochun Jiang, jiangxiaochun2019@hotmail.com.

CRediT authorship contribution statement

Chenhui Zhao: Writing – original draft, Methodology, Investigation, Funding acquisition, Data curation, Conceptualization. **Zeyu Wu:** Methodology, Investigation, Data curation. **Zhipeng Yao:** Methodology, Investigation, Validation, Resources. **Fan Zhang:** Investigation, Data curation, Bioinformatics analysis, Methodology. **Rui Zhao:** Methodology, Funding acquisition. **Xiaoxiang Cao:** Methodology. **Shizhang Ling:** Conceptualization, Methodology, Investigation, Data curation, Funding acquisition, Writing – review & editing. **Xiaochun Jiang:** Writing – review & editing, Supervision, Project administration, Investigation, Conceptualization.

Declaration of competing interest

The authors report no conflict of interest.

Acknowledgments

This work was supported by the funding of Wuhu Science and Technology Plan Project (2022jc69), Young and Middle-Aged Research Fund Project of Wannan Medical College (WK2021F22), Key natural science projects of Anhui Provincial Department of Education (2022AH051250), “Peak”Training Program for Scientific Research of The Affiliated Hospital of Wannan Medical College (PF2019003), and Anhui Excellent Scientific Research and Innovation Team (2022AH010073).

Appendix A. Supplementary data

Supplementary data to this article can be found online at https://doi.org/10.1016/j.heliyon.2024.e36597.

References

[1] L.M. Barrera, L.D. Ortiz, H.J. Grisales, M. Camargo, Survival analysis and associated factors of highgrade glioma patients, Biomedica 44 (2024) 191–206.
[2] C. McKinnon, M. Nandhabalan, S.A. Murray, P. Plaha, Glioblastoma: clinical presentation, diagnosis, and management, Bmj 374 (2021) n1560.
[3] E. Agosti, S. Antonietti, T. Ius, M.M. Fontanella, M. Zeppieri, P.P. Panciani, Glioma stem cells as promoter of glioma progression: a systematic review of molecular pathways and targeted therapies, Int. J. Mol. Sci. 25 (2024).
[4] V. Venkataramani, Y. Yang, M.C. Schubert, E. Reyhan, S.K. Tetzlaff, N. Wissmann, M. Botz, S.J. Soyka, C.A. Beretta, R.L. Pramatarov, L. Fankhauser, L. Garofano, A. Freudenberg, J. Wagner, D.I. Tanev, M. Ratliff, R. Xie, T. Kessler, D.C. Hoffmann, L. Hai, Y. Dorflinger, S. Hoppe, Y.A. Yabo, A. Golebiewska, S. P. Niclou, F. Sahm, A. Lasorella, M. Slowik, L. Doring, A. Iavarone, W. Wick, T. Kuner, F. Winkler, Glioblastoma hijacks neuronal mechanisms for brain invasion, Cell 185 (2022) 2899–2917 e2831.
[5] S. Schlieper-Scherf, N. Hebach, D. Hausmann, D.D. Azorin, D.C. Hoffmann, S. Horschitz, E. Maier, P. Koch, M.A. Karreman, N. Etminan, M. Ratliff, Disrupting glioblastoma networks with tumor treating fields (TTFields) in in vitro models, J. Neuro. Oncol. (2024), https://doi.org/10.1007/s11060-024-04786-0.
[6] T.N. Phoenix, The origins of medulloblastoma tumours in humans, Nature 609 (2022) 901–903.

[7] A.S. Plant-Fox, U. Tabori, Future perspective of targeted treatments in pediatric low-grade glioma (pLGG): the evolution of standard-of-care and challenges of a new era, Childs Nerv. Syst. (2024), https://doi.org/10.1007/s00381-024-06504-7.
[8] D. Killock, Extent of resection is important across glioblastoma molecular subtypes, Nat. Rev. Clin. Oncol. 17 (2020) 275.
[9] M.J. Goldman, A.M. Baskin, M.A. Sharpe, D.S. Baskin, Advances in gene therapy for high-grade glioma: a review of the clinical evidence, Expert Rev. Neurother. (2024) 1–17.
[10] J. Lin, T. Zhou, J. Wang, Solution structure of the human HSPC280 protein, Protein Sci. : a publication of the Protein Society 20 (2011) 216–223.
[11] R.B. Haga, A.J. Ridley, Rho GTPases: regulation and roles in cancer cell biology, Small GTPases 7 (2016) 207–221.
[12] S. Porazinski, A. Parkin, M. Pajic, Rho-ROCK signaling in normal physiology and as a key player in shaping the tumor microenvironment, Advances in experimental medicine and biology 1223 (2020) 99–127.
[13] T. Shibue, Visualizing the cell-matrix interactions and cytoskeleton of disseminated tumor cells, Methods Mol. Biol. 2811 (2024) 207–220.
[14] T.L. Pang, F.C. Chen, Y.L. Weng, H.C. Liao, Y.H. Yi, C.L. Ho, C.H. Lin, M.Y. Chen, Costars, a Dictyostelium protein similar to the C-terminal domain of STARS, regulates the actin cytoskeleton and motility, J. Cell Sci. 123 (2010) 3745–3755.
[15] B. Ura, L. Monasta, G. Arrigoni, C. Franchin, O. Radillo, I. Peterlunger, G. Ricci, F. Scrimin, A proteomic approach for the identification of biomarkers in endometrial cancer uterine aspirate, Oncotarget 8 (2017) 109536–109545.
[16] D. Wang, H. Liu, C. Ren, L. Wang, High expression of ABRACL is associated with tumorigenesis and affects clinical outcome in gastric cancer, Genet. Test. Mol. Biomarkers 23 (2019) 91–97.
[17] J. Li, H. Chen, Actin-binding Rho activating C-terminal like (ABRACL) transcriptionally regulated by MYB proto-oncogene like 2 (MYBL2) promotes the proliferation, invasion, migration and epithelial-mesenchymal transition of breast cancer cells, Bioengineered 13 (2022) 9019–9031.
[18] B.Y. Hsiao, C.H. Chen, H.Y. Chi, P.R. Yen, Y.Z. Yu, C.H. Lin, T.L. Pang, W.C. Lin, M.L. Li, Y.C. Yeh, T.Y. Chou, M.Y. Chen, Human costars family protein ABRACL modulates actin dynamics and cell migration and associates with tumorigenic growth, Int. J. Mol. Sci. 22 (2021).
[19] S. Fan, P. Chen, S. Li, miR-145-5p inhibits the proliferation, migration, and invasion of esophageal carcinoma cells by targeting ABRACL, BioMed Res. Int. 2021 (2021) 6692544.
[20] M. Wang, X. Jiang, Y. Yang, H. Chen, C. Zhang, H. Xu, B. Qi, C. Yao, H. Xia, Rhoj is a novel target for progression and invasion of glioblastoma by impairing cytoskeleton dynamics, Neurotherapeutics : the journal of the American Society for Experimental NeuroTherapeutics 17 (2020) 2028–2040.
[21] R. Mikyskova, O. Sapega, M. Psotka, O. Novotny, Z. Hodny, S. Balintova, D. Malinak, J. Svobodova, R. Andrys, D. Rysanek, K. Musilek, M. Reinis, STAT3 inhibitor Stattic and its analogues inhibit STAT3 phosphorylation and modulate cytokine secretion in senescent tumour cells, Mol. Med. Rep. 27 (2023).
[22] A.C. Tan, D.M. Ashley, G.Y. Lopez, M. Malinzak, H.S. Friedman, M. Khasraw, Management of glioblastoma: state of the art and future directions, CA: a cancer journal for clinicians 70 (2020) 299–312.
[23] E. Stylianopoulou, G. Kalamakis, M. Pitsiani, I. Fysekis, P. Ypsilantis, C. Simopoulos, G. Skavdis, M.E. Grigoriou, HSPC280, a winged helix protein expressed in the subventricular zone of the developing ganglionic eminences, inhibits neuronal differentiation, Histochem. Cell Biol. 145 (2016) 175–184.
[24] C.J. Pirozzi, H. Yan, The implications of IDH mutations for cancer development and therapy, Nat. Rev. Clin. Oncol. 18 (2021) 645–661.
[25] J.E. Eckel-Passow, D.H. Lachance, A.M. Molinaro, K.M. Walsh, P.A. Decker, H. Sicotte, M. Pekmezci, T. Rice, M.L. Kosel, I.V. Smirnov, G. Sarkar, A.A. Caron, T. M. Kollmeyer, C.E. Praska, A.R. Chada, C. Halder, H.M. Hansen, L.S. McCoy, P.M. Bracci, R. Marshall, S. Zheng, G.F. Reis, A.R. Pico, B.P. O'Neill, J.C. Buckner, C. Giannini, J.T. Huse, A. Perry, T. Tihan, M.S. Berger, S.M. Chang, M.D. Prados, J. Wiemels, J.K. Wiencke, M.R. Wrensch, R.B. Jenkins, Glioma groups based on 1p/19q, IDH, and TERT promoter mutations in tumors, N. Engl. J. Med. 372 (2015) 2499–2508.
[26] H. Yan, D.W. Parsons, G. Jin, R. McLendon, B.A. Rasheed, W. Yuan, I. Kos, I. Batinic-Haberle, S. Jones, G.J. Riggins, H. Friedman, A. Friedman, D. Reardon, J. Herndon, K.W. Kinzler, V.E. Velculescu, B. Vogelstein, D.D. Bigner, IDH1 and IDH2 mutations in gliomas, N. Engl. J. Med. 360 (2009) 765–773.
[27] K. Arney, Improving brain-cancer therapies through mathematical modelling, Nature 561 (2018) S52–S53.
[28] K. Anderson, Y. Calle-Patino, A. Ivetic, M. Parsons, F. Valderrama, C. Wells, I. Anton, Cell adhesion and migration in disease: translational and therapeutic opportunities, Cell Adh Migr 18 (2024) 1–3.
[29] H.K. Matthews, C. Bertoli, R.A.M. de Bruin, Cell cycle control in cancer, Nat. Rev. Mol. Cell Biol. 23 (2022) 74–88.
[30] A. da Costa, D. Chowdhury, G.I. Shapiro, A.D. D'Andrea, P.A. Konstantinopoulos, Targeting replication stress in cancer therapy, Nat. Rev. Drug Discov. 22 (1) (2023) 38–58.
[31] C. Zhao, X. Fan, W. Gao, F. Zhang, H. Lv, X. Jiang, G. Di, De-differentiation associated with drop metastasis of a recurrent intracranial solitary fibrous tumor: a case report and literature review, Int. J. Neurosci. 132 (2022) 843–849.
[32] T.R. Cox, The matrix in cancer, Nat. Rev. Cancer 21 (2021) 217–238.
[33] K. Dvorakova, V. Skarkova, B. Vitovcova, J. Soukup, H. Vosmikova, Z. Pleskacova, A. Skarka, M.C. Bartos, P. Krupa, P. Kasparova, J. Petera, E. Rudolf, Expression of STAT3 and hypoxia markers in long-term surviving malignant glioma patients, BMC Cancer 24 (2024) 509.
[34] D. Yu, S. Wang, J. Wang, K. Zhang, Z. Niu, N. Lin, EZH2-STAT3 signaling pathway regulates GSDMD-mediated pyroptosis in glioblastoma, Cell Death Discov 10 (2024) 341.
[35] S. Kumar, D.A. Arwind, B.H. Kumar, S. Pandey, R. Nayak, M.P. Vithalkar, N. Kumar, K.S.R. Pai, Inhibition of STAT3: a promising approach to enhancing the efficacy of chemotherapy in medulloblastoma, Transl Oncol 46 (2024) 102023.